Large Scale Unconfined Gasoline Spray Detonation

Fan Zhang[1], Richard Findlay[1], John Anderson[1], and Robert Ripley[2]
[1]Defence R&D Canada – Suffield, Medicine Hat, AB, Canada
[2]Martec Ltd., Halifax, NS, Canada

1 Introduction

Large scale experiments on unconfined detonation of motor fuel sprays or solid particles in air provide valuable fundamental data. These include detonation in: semi-cylindrical clouds of gasoline or kerosene spray, 1100–1500 m^3 in volume and 3–8 m in radius [1-2]; explosive-dispersed spray clouds from a gasoline, kerosene or diesel fuel canister of 0.1 to 100 metric tons [3-4]; and quarter-cylindrical aluminum particle clouds, 230 m^3 in volume and 4 m in radius [5]. The results show that the gasoline spray detonation, after a sufficiently long suspension time, requires a critical initiation TNT charge mass of 0.64 kg [1-2]. As the suspension time is reduced, the critical initiation charge mass increases towards a few kilograms. In contrast, the critical initiation charge mass is 4.5 kg for kerosene spray detonation [1] and 5 to 8 kg for flake and 2–3 μm atomized aluminum-air detonation [5]. The critical blast radius is reported to be R_C = 2.75 m ≈ 55 λ for the gasoline-air [2], and R_C = 10 m ≈ 20 λ for the aluminum-air where λ is the detonation cell width [5]. The smaller critical initiation charge mass and detonation cell width for gasoline indicates that the detonation at a sufficiently long spray suspension time is controlled by the vapour phase. The fact that kerosene has the same order of the critical initiation charge mass as that of aluminum particles would suggest the dominance of liquid droplets in heterogeneous detonation of low vapour pressure fuels.

In the present paper, a much larger scale (more than 70,000 m^3) unconfined gasoline spray detonation has been experimentally investigated to examine the detonation performance and scale effect. Particulate jetting instabilities from explosive dispersal of bulk liquid has been further explored experimentally and numerically to study the possible mechanisms for the droplet jet formation.

2 Experimental Methodology

The detonation experiment in the present investigation was carried out in an explosively dispersed spray cloud from a fuel canister configuration. 7103 liters of gasoline (clear primary without ethanol supplied by Petro Canada) was contained within a polyethylene-walled cylindrical container, 1.6 m in inner diameter as given in Fig. 1. The density of gasoline was measured to be 0.717 g/cm^3 which results in a total test fuel weight of 5093 kg. The gasoline was dispersed using a centrally located cylindrical explosive burster charge within a thin-walled hard PVC tube, where the burster charge was detonated from the top with an exploding wire RP83 detonator (0.08 g PETN plus 1.031 g RDX). The gasoline charge had a 5.75 m height of burst which defines the distance from the charge center to the ground level. In order to directly initiate the detonation of dispersed gasoline spray, an appropriately

Correspondence to: fan.zhang@drdc-rddc.gc.ca

massed secondary charge was used and located at a radius R = 20 m from the gasoline canister at 45° between the east and the north radial line. An additional tertiary charge was placed at R = 30 m from the gasoline canister at 45° between the north and the west radial line. The tertiary charge ensured the direct initiation of detonation in case the secondary charge failed. Both the secondary and tertiary charges have a height of burst of 1.5 m, initiated from the charge top using a RP83 detonator.

Fig. 1 Gasoline canister in filling

Pressures and impulses were measured using ground level rail-style gauge mounts with Kulite piezo-resistance transducers, which were located 5.5 m, 8 m, 10.5 m, 13 m, 15.5 m, 18 m, 20.5 m, 23 m, 25.5 m, 28 m, 33 m, 38 m, 43 m, 48 m, 53 m, 60 m, 70 m, 80 m, 120 m, 160 m, 200 m, 350 m and 1300 m (a PCB piezo-electric transducer) from the primary gasoline charge center in the west radial line and 5 m, 10 m, 15 m, 18 m, 19 m, 20 m, 21 m, 22 m, 30 m, 40 m, 50 m, 60 m, 70 m and 80 m in the north radial line. Flame temperatures were measured using Omega C-Type thermocouples (calibrated up to 2200 °C) installed in two radial lines between 10 and 39m. The thermocouples have a slow response time on the order of milliseconds and therefore provide a history of ms-averaged fireball temperature. High-speed video cameras were employed to record the geometry and process of the event and they were mounted at a west and a north location facing the gasoline charge.

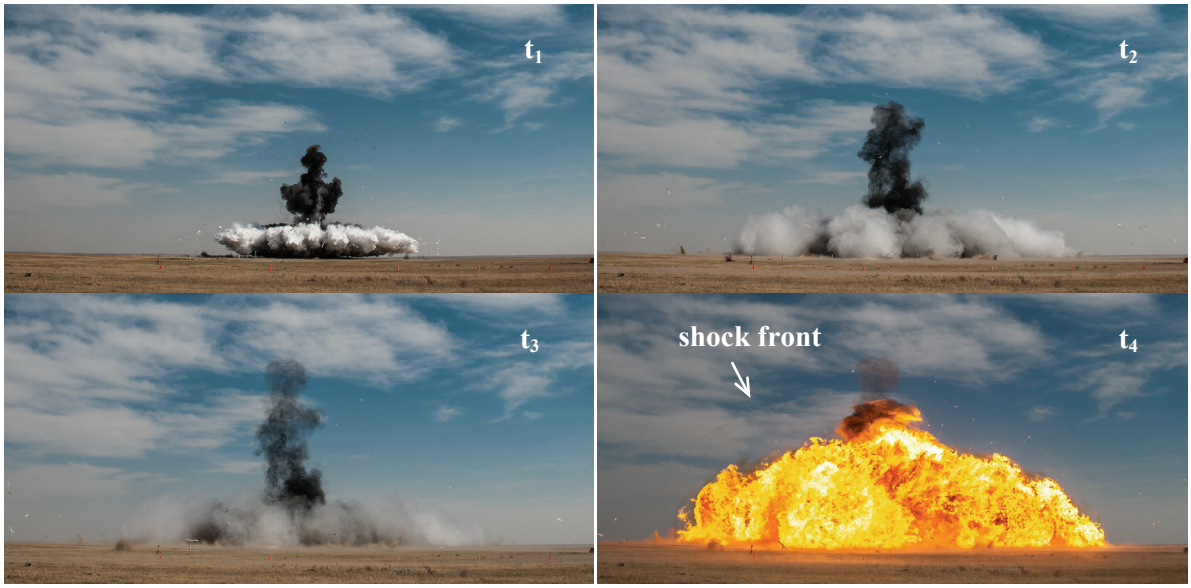

Fig. 2 Gasoline spray dispersal, evaporation and detonation

The gasoline spray-air mixture was prepared through explosive dispersal using a centrally located cylindrical explosive burster charge, as shown in Fig. 2 taken from the west high-speed video (2000 frames/s). Detonation of the burster charge causes the gasoline liquid to expand, fragment and form the droplet jets spreading outwards (see the photograph at t_1). The beginning of the evaporation of the liquid fuel can be identified through a temperature drop about 15-20 °C in the thermocouple records. The vapor phase becomes visible at t_2 while the merging of small jets also takes place partially due to the aerodynamic forces. The formed fuel vapor partially fills the air gaps between the jets (t_3) while the inertia causes the fuel spray jets to further move outwards. Note that the wind speed is 15-30 km/h from southwest, the cloud radius of the north jet (the left side of photos in Fig. 2) is therefore greater

than that of the south jet (the right side of photos in Fig. 2) in the late times. Immediately prior to detonation, the cloud radius and height are R = 43.3 m and H = 12.7 m, thus resulting in a cloud volume $\pi R^2 H$ = 74766 m^3. Primary gasoline is typically composed of iso-octane, heptanes, cyclo-pentane, ethyl-benzene and butane. Assuming that the total mass of the gasoline was made of iso-octane, at the local air pressure 92.46 kPa and temperature 28 °C the volume for the stoichiometric fuel-air mixture would take 71570 m^3 if the fuel stays in full liquid form and 72777 m^3 if the fuel is in the full vapor phase. The mean volume between the liquid and vapor phase values divided by the experimental volume 74766 m^3 equals 0.9653. Noticing the air gaps between the fuel spray jets at the larger radii, a near stoichiometric fuel-air mixture in average is preserved when the cloud is detonated. At a sufficient suspension time, detonation of the secondary and tertiary charges leads to the direct initiation of detonation of the spray cloud. The last photograph in Fig. 2 (t_4) shows the intense blast with a leading shock wave followed by the fireball after the successful cloud detonation.

3 Detonation Results

Figure 3 shows some typical overpressure histories at 13 m, 18 m, 23 m and 28 m in the west radial line, where the front peak overpressure ranges between 1.70 and 1.86 MPa ($\Delta p/p_0$ = 18.4-21.2). The arrival times of the wave front for these four gauge locations are 13.1 ms, 12.5 ms, 12.3 ms and 13.5 ms, respectively, with respect to the detonation initiation instant. These arrival times indicates a piece of spherical detonation front propagating approximately from north to south, which is initiated from the tertiary charge center at R = 30 m, 45° from the north and west radial lines. The detonation front has an average velocity of 1900 m/s derived from its arrival between the west radial line and near the south edge of the cloud using the high-speed video records. Note that a pressure peak appears behind the front at about 24.5 ms in the pressure history at 13 m in Fig. 3. This peak can be traced back to the wave generated through the collision of the two detonation waves initiated by the secondary charge and the tertiary charge, respectively. This wave can be further identified in the other transducer locations in later times with the propagation distance (29 ms at 18 m, 33 ms at 23 m and 37 ms at 28 m).

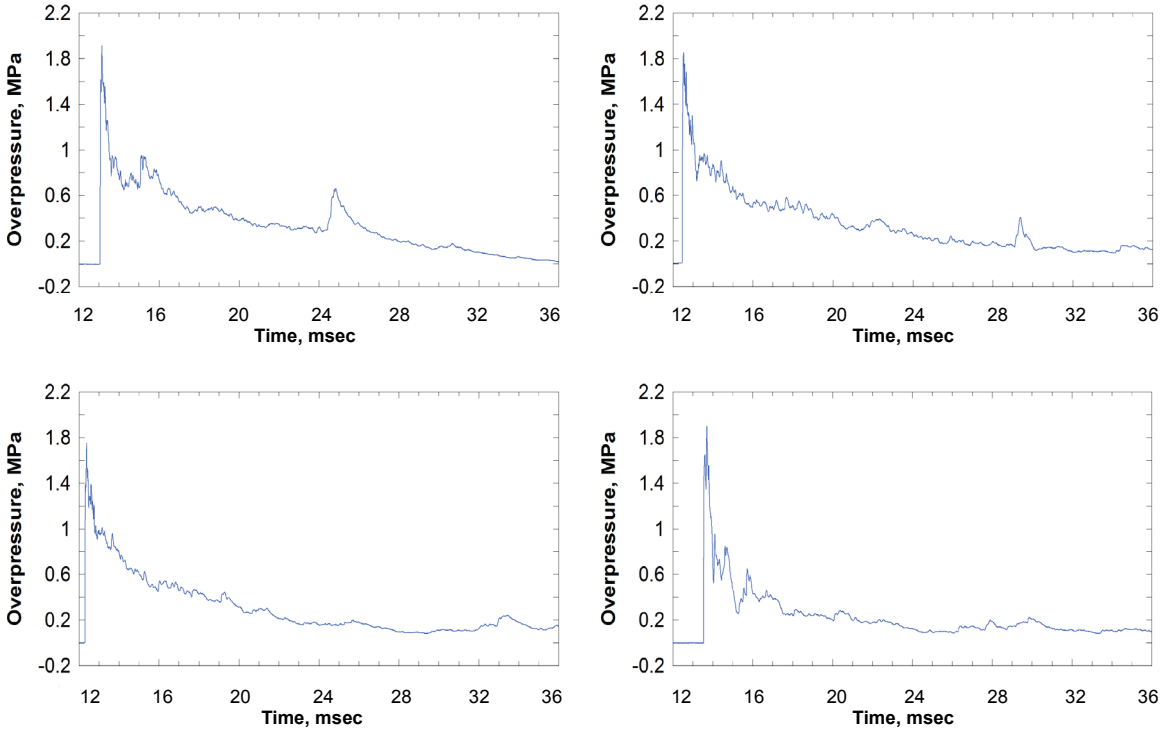

Fig. 3 Overpressure histories at gauges 13 m, 18 m, 23 m and 28 m in the west radial line

Figure 4 summarizes the wave front peak overpressures and maximum impulse at all ground-level gauges along both the west and north lines. The overpressure and impulse profiles show a plateau with the values mostly in the range of 1.70-2.17 MPa ($\Delta p/p_0$ = 18.4-23.5) and 7.26-13.3 MPa-ms. This plateau indicates the detonation area with a radius of 40-43 m, in agreement with the high-speed video result (R ≈ 43 m). Note that in the literature [1-2], Alekseev et al. measured a detonation velocity between 1500 and 1800 m/s and detonation overpressures between 1.5 and 1.8 MPa. Both the detonation velocity and overpressure in the present study are higher. The overpressure and impulse values versus radius after the detonation plateau in Fig. 4 display the performance of the decaying blast wave as it propagates up to 1.3 km (about 30 cloud radii).

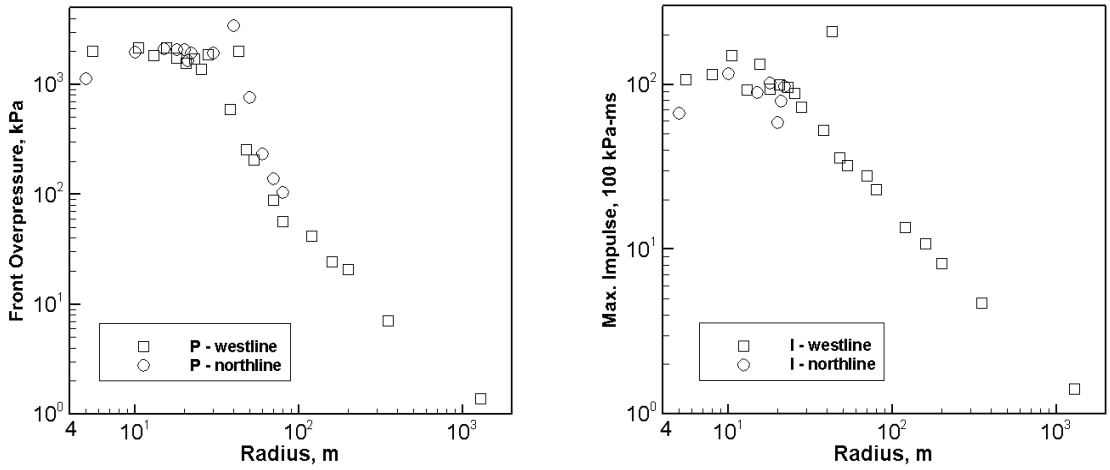

Fig. 4 Front overpressure and maximum impulse of gasoline spray detonation and subsequent blast

The cellular structure of the gasoline spray detonation has been traced at the ground area of fine soil particles which were generated due to a number of large scale trials conducted before this gasoline spray detonation trial. Figure 5 provides an example of such records; the measured average detonation cell width from these records is 6.8±1.4 cm. This result is in agreement with the original records by Alekseev et al. (λ = 3.6-10 cm measured from the three smoke foils likely from the different locations of the non-uniform cloud in [2]), and with the cell widths (λ = 5.4-6.7 cm) measured by Knystautas et al. for the stoichiometric, alkane gas (C_2H_6, C_3H_8 or C_4H_{10}) fuel-air mixtures in laboratory detonation tubes [6].

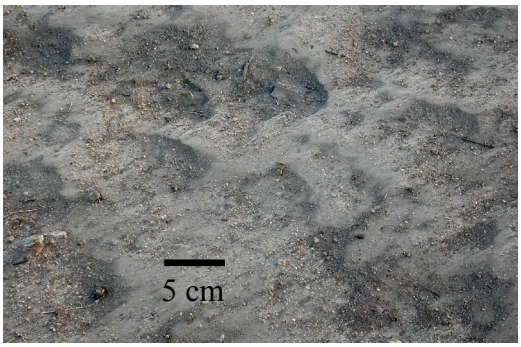

Fig. 5 A fine soil particle ground record of the cellular structure of gasoline spray detonation

The peak fireball temperatures received from all the thermocouple gauges along both the near-west and near-north lines were between 1400 and 1650 K; the measured temperatures shall be interpreted as the fireball temperatures after the detonation due to the slow response time of the thermocouples.

4 Jetting Instabilities from Explosive Dispersal

When bulk liquid or a packed bed of metallic particles is explosively dispersed, incipient instabilities develop visibly on the surface, forming filaments consisting of clusters of droplets or particles. At higher dispersal speeds, the droplet or particle cloud is highly perturbed and coherent jet structures form very early during the expansion [7-11].

The mechanisms for the formation of these instabilities or jets remain as an up-to-date research topic in the area of high speed dense particle flow. Milne et al. pointed out that the Rayleigh Taylor instability, which takes long time to develop, was unlikely the cause of the formation of jet structures [7]. Frost et al. postulated that the breakup of a layer of particles at high strain rates is also governed by a balance of expansion inertia effects tending to fracture a layer of particles versus viscous dissipation which will tend to maintain the stability of the layer [8]. An analysis of trial data from cylindrical explosive dispersal of either a pure liquid, dry solid particles or a mixture of both indicates that the incipient number of particle jets is mainly dominated by the initial particle expansion velocity [9-10]. The experimental initial particle expansion velocity was found to be in good agreement with the so-called "Gurney velocity", which was determined by the mass ratio of the packed particle bed to the explosive. Once the jet forms, aerodynamic forces tend to stabilize or merge the jets as they propagate over large distances. Using mesoscale simulations, Xu et al. indicated that jet-like gas instabilities developed at the interface between the center explosive and the surrounding packed particle bed and determined the maximum number of particle jets formed [11]. In summary, the mechanisms for the formation of jet structures appear due to the instabilities near the interface between the driver explosive and the packed particle bed or/and the instabilities near the interface of outer edge of the packed bed and air; both interfaces can entail thin-walled casings.

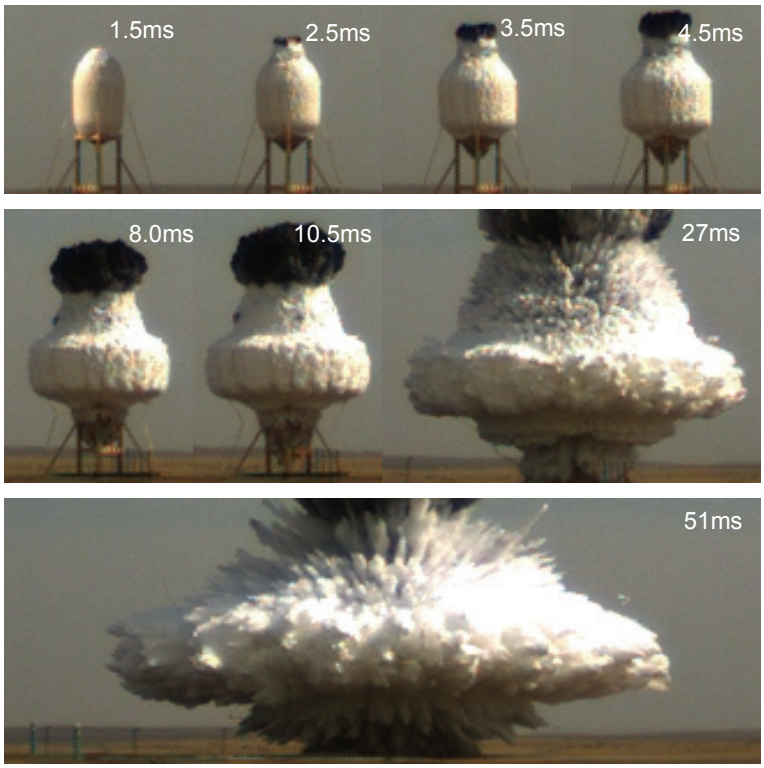

Fig. 6 Early process of gasoline liquid dispersal: liquid break-up, fragmentation and jet formation

Figure 6 shows the high-speed photographic records of the early time dispersal of gasoline in the present experiment. Based on the arguments in the previous paragraph, it is of interest to see what the stability of the liquid depends on. In the photographs, the polyethylene casing starts to fragment longitudinally along the casing length once expanded between 1.5-2 times the initial diameter. Afterwards the small disturbances can be identified on the entire surface of the casing and develop into fine fragments followed by small liquid jets. The fractures through the bulk liquid are visible after 8 ms, traced back to the main longitudinal fragment locations. The main spray jet structures are

developed between the radial fractures through the bulk liquid (see the photos at 27 ms and 51 ms and late times in Fig. 2), while small spray jets overlap on these main jet structures. Since the radial fractures of bulk liquid occur incipiently as evidenced by the longitudinal fragmentation of the casing, one would postulate that the formation of the coherent jets must be related to the cumulative instabilities at the interface between the driver explosive and bulk liquid entailing the fragmentation of the thin-walled PVC casing containing the driver explosive. The maximum number of main jets could then be associated with the fragment number of this inner casing, in agreement with the conclusion drawn from the meso-scale simulations in [11].

Macro-scale numerical modeling has been conducted to simulate the above observations and further validate the mechanism postulated. The simulation modeled a down-scaled cylindrical charge 100 mm in diameter containing water (ρ = 1 g/cc) with a 10 mm diameter central burster of TNT (ρ = 1.6 g/cc). A 2D planar domain was used to represent the cross-section of a long cylindrical charge, while symmetry planes were employed to represent one-quarter of the charge circumference. The explosive was centrally initiated with a cylindrical detonation propagating outwards. The interior liquid-explosive boundary featured a thin pre-fragmented casing (steel, 0.9 mm thick). The early shock dynamics including detonation and shock transmission into the bulk liquid were calculated on an Eulerian mesh using continuum material models. The burster TNT was represented by a Mie-Grüneisen equation of state (EOS) and the JWL EOS was used for its detonation products. The Tait EOS was used for the water in compression followed by an isentrope under small tension. A closely-coupled fluid-structure interaction capability was used for the burster casing fragments in which a conservative locally-adaptive mesh approach was used. The CFD mesh was unstructured quadrilateral elements 0.2 mm in size; the casing structural elements were also 0.2 mm. Within the quarter-symmetric model, the buster casing was pre-failed at four equally-spaced points, representing 17 fragments around the entire circumference. The liquid shock in water reached the outer boundary (air interface) at 20 us and reflects as an expansion wave travelling inwards. Bulk breakup of the liquid was assumed for pressure below 5000 Pa, equivalent to a liquid strain of 0.006. A group Lagrange approach was used for the droplets, where each 'particle' group represented a collection of physical droplets. The majority of droplets had a mean size of 120 μm (size distribution from 26-307 μm). The denser liquid compressed by the detonation products was later fragmented at a fixed time of 50 μs into a prescribed size distribution with a mean of 250 μm (ranging from 58-490 μm). In this calculation, a total of 210,519 droplet groups were created. The 'particle' dynamics were computed using a simple drag law as a function of Reynolds number alone. A series of remapping steps were performed on successively larger meshes, with the final resolution being 60 mm at 15 m radius. The above capabilities have been implemented in the Chinook CFD code developed by Martec Limited and Defence Research and Development Canada.

Figure 7 displays the numerical results of the dispersal process. As the explosive detonation reaches the surface of the burster casing, the five casing fragments start to move outwards within the quarter-symmetical domain. A fragment moves faster than the neighboring liquid due to the inertia and is accompanied with a high-pressure detonation products gas jet behind, thus resulting in a compressed liquid strip surrounded (Fig. 7 at 50 μs). At this moment the fragments have a velocity greater than 650 m/s while the velocity of the liquid at the same radius is about 250-300 m/s (note that the shock front is already transmitted into the air out of the domain in the figure). The high-pressure gas jets squeeze the liquid between them, while the leading edges of the compressed liquid strips in front of the five fragments exhibit the highest circumferential strain and therefore become the liquid surface fracture points as the fragments move towards the outer surface of the liquid. The four squeezed liquid strips between these fracture points are marked as the arrows in the later times (Fig. 7 at 4 ms), where the majority of liquid breaks into droplets due to the tension. The squeezed strips of liquid and droplet particles between the gas jets move outwards driven by the outward force component of neighboring high-pressure gas. Due to the velocity difference, the squeezed particles move faster than and eventually overtake the discrete particles in the neighboring gas jets, as evidenced in Fig. 7 at 10 ms, where the innermost layer of the squeezed particles already move ahead of the particles in the

original gas jets. This finally leads to the formation of the coherent particle jets between the radial surface fracture points of the liquid as shown in the last picture of Fig. 7. The main particle jet number is therefore determined by the liquid radial fracture points which are controlled by the fragment number of the burster casing between the burster explosive and the bulk liquid. Thus, the numerical simulation is in agreement with the experimental observation about the consistency of main particle jet number with the bulk liquid radial surface fractures, and has further explored in detail that the formation of the fractures and main particle jets is originated in the interface perturbations of the burster explosive and the bulk liquid.

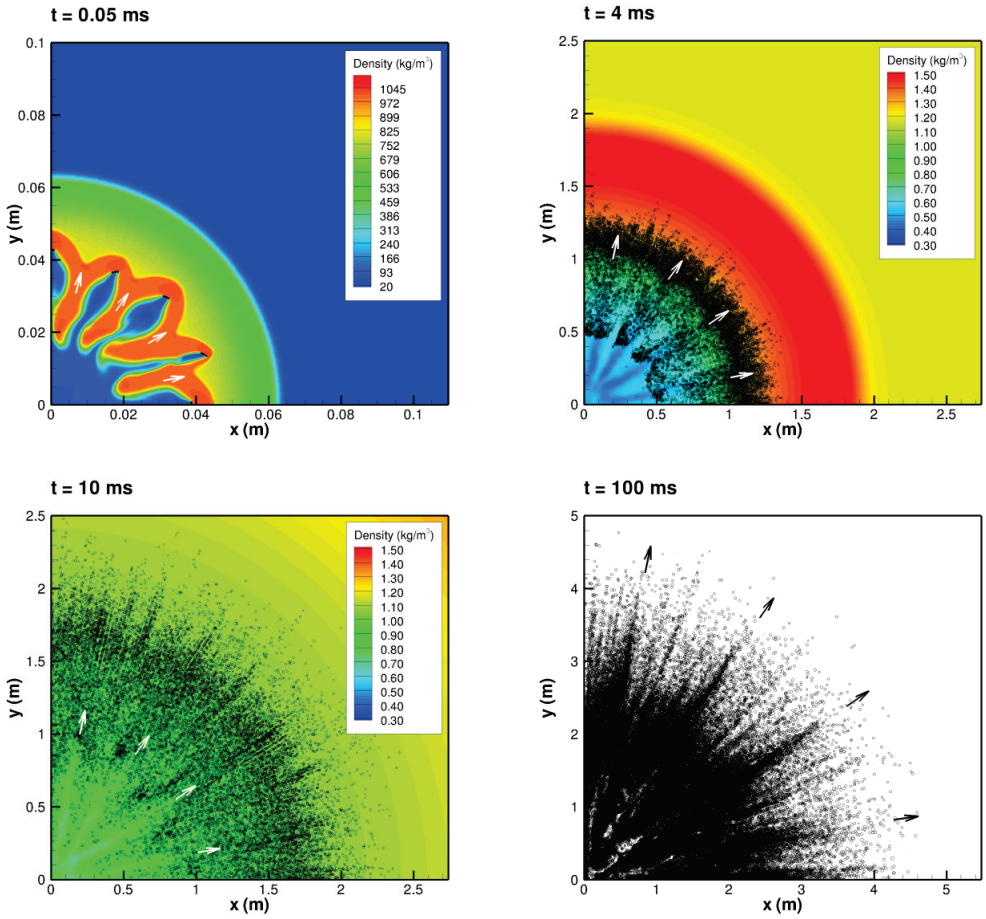

Fig. 7 Modeling of liquid dispersal: liquid fragmentation and droplet jet formation

5 Conclusions

A large scale experiment of unconfined detonation of 7103 L gasoline spray in air has been successfully conducted through the explosive dispersal approach. The detonation observed has a mean velocity of 1900 m/s and overpressure in the range of 1.70-2.17 MPa ($\Delta p/p_0$ = 18.4-23.5), with a mean detonation cell width of 6.8±1.4 cm. Explosive dispersal of bulk gasoline liquid leads to the formation of a spray cloud consisting of a number of particle jet structures that remain coherent after travelling for many charge diameters. The radial fractures through the bulk liquid surface and formation of the coherent jet structures are likely caused by the perturbations of the interface between the driver explosive and bulk liquid involving the fragmentation of the casing containing the explosive, while the instabilities of the interface between the outer edge of the bulk liquid and air entailing the

fragmentation of the casing containing the bulk liquid further generate fine jets overlapping on the main jet structures. Macro-scale numerical simulation obtains a more mechanistic description, in which the high-pressure detonation products gas jets, induced from the casing fragments at the interface between the driver explosive and bulk liquid, squeeze the liquid strip between the gas jets. The squeeze of the liquid strip leads to the formation of the main droplet jets between the radial surface fracture points of the bulk liquid. In order to enable the numerical modeling more quantitatively, the models for the fracture of bulk liquid and the interactions in the subsequent dense particle flow will be further improved.

Acknowledgements

The authors would like to thank Brain Eichelbaum, Kiril Mudri, Robin Lien, Darrell Boechler, Mark Churcher, Karl Baker and the technical staff from the Suffield Field Operations Section for their significant effort and support in conducting the experiments, Chris Cloney and Scott McClennan for numerical model development, and Dr. Stephen Murray and Dr. Paul Thibault for useful discussions.

References

[1] Alekseev, V.I., Dorofeev, S.B., Sidorov, V.P., Chaivanov, B.B. (1993). Experimental study of large-scale unconfined fuel spray detonations. In: Progress in Astronaut. Aeronaut., vol. 154, AIAA, Reston, pp. 95–104.

[2] Alekseev V.I., Dorofeev, S.B., Sidorov, V.P. (1996). Direct initiation of detonations in unconfined gasoline sprays. Shock Waves 6: 67.

[3] Dorofeev, S.B. (1995). Blast effects of confined and unconfined explosions. In: Proc. 20th Int. Symp. on Shock Waves, Pasadena, pp. 77–86.

[4] Dorofeev, S.B., Sidorov, V.P., Kuznetsov, M.S., Dvoinishnikov, A.E., Alekseev, V.I., Efimenko, A.A. (1996). Air blast and heat radiation from fuel-rich mixture detonations. Shock Waves 6: 21.

[5] Zhang, F., Gerrard, K., Ripley, R.C. (2009). Reaction mechanism of aluminum particle-air detonation. J. Propulsion and Power 25: 845.

[6] Knystautas, R., Guirao, C., Lee, J.H., Sulmistras, A. (1984). Measurements of cell size in hydrocarbon-air mixtures and predictions of critical tube diameter, critical initiation energy, and detonability limits. In: Progress in Astronaut. Aeronaut., vol. 94, AIAA, New York, pp. 23–37.

[7] Milne AM, Parrish C, Worland I. (2010). Dynamic fragmentation of blast mitigants. Shock Waves 20: 41.

[8] Frost, D.L., Gregoire, Y., Goroshin, S., Zhang, F. (2011). Interfacial instabilities in explosive gas-particle flows. In: Proc. 23rd ICDERS, Irvine.

[9] Zhang F, Yoshinaka A, Ripley R. (2010). Hybrid detonation waves in metalized explosive mixtures. In: Proc. 14th Int. Detonation Symp. Coeur d'Alene, Idaho, pp. 714-723.

[10] Ripley, R.C., Donahue, L., Zhang, F. (2011). Jetting instabilities of particles from explosive dispersal. Shock Compression of Condensed Matter – 2011, pp. 1615-1618.

[11] Xu, T., Lien, F.-S., Ji. H., Zhang, F. (2013). Formation of particle jetting in a cylindrical shock tube. Shock Waves (accepted).